PERGAMON

International Journal of Plasticity 19 (2003) 2121–2147

INTERNATIONAL JOURNAL OF Plasticity

www.elsevier.com/locate/ijplas

Thermodynamic based model for the evolution equation of the backstress in cyclic plasticity

George Z. Voyiadjis*, Rashid K. Abu Al-Rub

Civil and Environmental Engineering Department, Louisiana State University, Baton Rouge, LA 70803, USA

Received in final revised form 30 September 2002

Abstract

A nonlinear kinematic hardening rule is developed here within the framework of thermodynamic principles. The derived kinematic hardening evolution equation has three distinct terms: two strain hardening terms and a dynamic recovery term that operates at all times. The proposed hardening rule, which is referred in this paper as the FAPC (Fredrick and Armstrong–Phillips–Chaboche) kinematic hardening rule, shows a combined form of the Frederick and Armstrong backstress evolution equation, Phillips evolution equation, and Chaboche series rule. A new term is incorporated into the Frederick and Armstrong evolution equation that appears to have agreement with the experimental observations that show the motion of the center of the yield surface in the stress space is directed between the gradient to the surface at the stress point and the stress rate direction at that point. The model is further modified in order to simulate nonproportional cyclic hardening by proposing a measure representing the degree of nonproportionality of loading. This measure represents the topology of the incremental stress path. Numerically, it represents the angle between the current stress increment and the previous stress increment, which is interpreted through the material constants of the kinematic hardening evolution equation. This new kinematic hardening rule is incorporated in a material constitutive model based on the von Mises plasticity type and the Chaboche isotropic hardening type. Numerical integration of the incremental elasto-plastic constitutive equations is based on a simple semi-implicit return-mapping algorithm and the full Newton–Raphson iterative method is used to solve the resulting nonlinear equations. Experimental simulations are conducted for proportional and non-proportional cyclic loadings. The model shows good correlation with the experimental results.

Keywords: Nonlinear kinematic hardening rule; Thermodynamic principles; Non-proportional loading; Cyclic loading

* Corresponding author. Tel.: +1-225-578-8668; fax: +1-225-578-9176.
E-mail address: voyiadjis@eng.lsu.edu (G.Z. Voyiadjis).

0749-6419/03/$ - see front matter
doi:10.1016/S0749-6419(03)00062-7

1. Introduction

A vast number of models of varying level of sophistication have been developed to model the elasto-plastic behavior of metals under cyclic conditions. Major classes of these models include internal state variable theories (e.g. Dafalias and Popov, 1975, 1976; Chaboche and Rousselier, 1981, 1983; Lemaitre and Chaboche, 1990; Dornowski and Perzyna, 1999, 2000) and multisurface models (e.g. Mroz, 1967; Krieg, 1975; Ohno, 1982; Tseng and Lee, 1983; McDowell, 1985a, b; Voyiadjis and Kattan, 1990; Voyiadjis and Sivakumar, 1991). The major difference among these different plasticity models available in the literature is the hardening rules which describe the movement of the yield surface corresponding to the kinematic hardening and the change in the size of the yield surface corresponding to the isotropic hardening. The loading surface separates the elastic and plastic response regions, which is characterized by its center and radius represented by the backstress and inner yield strength, respectively.

Isotropic hardening (Hill, 1950) and/or kinematic hardening (Prager, 1956) are commonly used concepts to describe the plastic behavior of the class M materials (metal-like behavior) under complex loading conditions. In classical theories of plasticity, the yield condition is expressed as a von Mises type:

$$f = J(\boldsymbol{\tau} - \boldsymbol{X}) - R(p) \equiv 0, \tag{1}$$

where $J(\boldsymbol{\tau} - \boldsymbol{X})$ is the second invariant of the deviatoric stress $\boldsymbol{\tau} - \boldsymbol{X}$, $\boldsymbol{\tau}$ and $\boldsymbol{X}$ are second-order tensors indicating the deviatoric component of the Cauchy stress and the translation of the yield surface, respectively, and p is a scalar proportional to the effective plastic strain or the plastic work. Regarding the translation of the yield surface, Prager (1956) and Ziegler (1959) initiated the fundamental frame-work for kinematic hardening rules. The major difference of the two models is mainly the direction of the translation of the center of the yield surface in the reduced stress space. Mroz (1967, 1969) introduced the notion of a field of work-hardening moduli represented by a number of hypersurfaces, termed the loading surfaces. In the generalization of his model to non-proportional loading, a new rule for kinematic hardening is proposed that is different from that suggested by Prager (1956). Later Mroz et al. (1976) generalized the rule of Prager (1956) and that of Eisenberg and Phillips (1968) to express the phenomena of cyclic relaxation and cyclic creep. The Armstrong and Frederick (1966) nonlinear kinematic hardening rule generalized the Prager linear hardening rule by adding an evanescent strain-memory term (dynamic recovery term) for more accurate prediction of the multiaxial Bauschinger effect. The Armstrong and Frederick rule has been used extensively by Chaboche and Rousselier (1981, 1983) and Chaboche (1986, 1989, 1991), where an additive decomposition of the evolution equation of the backstress into several components of the Armstrong–Frederick type has been postulated. This decomposition shows an excellent correlation with the experimental results for monotonic and cyclic loading (e.g. Ohno and Wang, 1994; Voyiadjis and Basuroychowdhary, 1998; Abdel and Ohno, 2000; Bari and Hassan, 2002; Yoshida et al., 2002; Chun et al., 2002a, b). Recently, nonlinear kinematic hardening of the Frederick and Armstrong type have

been used and modified also by many authors (e.g. Duszek and Perzyna, 1991; Ohno and Wang, 1993a, b; Jiang and Kurath, 1996; Wang and Barkley, 1998, 1999; Abdel and Ohno, 2000, Voyiadjis and Basuroychowdhary, 1998; Basuroychowdhury and Voyiadjis, 1998; Geng and Wagoner, 2000; Bari and Hassan, 2002; Yaguchi et al., 2002).

Translation rules based on the concept of the bounding surface in the stress space were also proposed. The bounding surface is a stress surface located outside the yield surface (Krieg, 1975; Dafalias and Popov, 1975, 1976). Expansion of the bounding surface represents the development of isotropic hardening, while translation of the yield surface inside the bounding surface describes the nonlinear kinematic hardening (Ohno et al., 1989). The cyclic plasticity material models that are based on the concept of a two-surface plasticity model fail to account for the phenomena of complex material memory. The only contribution to the memory is through the initial and current proximity parameters from the yield surface (Voyiadjis and Basuroychowdhary, 1998; Basuroychowdhury and Voyiadjis, 1998). Tseng and Lee (1983) proposed a kinematic hardening rule based on the bounding surface concept which gives a better correlation with the experimental results. They assumed that the motion of the yield surface is directed between the deviatoric stress rate direction and the normal to the yield surface at the current loading point. The yield surface rotates when the yield surface is verging on contact with the bounding surface so that no intersection occurs between the yield surface and the bounding surface at the time of contact. Ohno and Wang (1991a) showed that the rate of the backstress as given by Chaboche (1989, 1991) is a multi-surface model. Ohno and Wang (1991b, 1993a, b, 1994) included in their model the hysterisis loop closure, ratcheting, dynamic recovery, static (thermal) recovery, and a temperature-rate term.

Voyiadjis and Basuroychowdhary (1998) and Basuroychowdhury and Voyiadjis (1998) proposed a two-surface plasticity model using a time dependent non-linear kinematic hardening rule to predict the non-linear behavior of metals under monotonic and non-proportional loadings. The model is based on Chaboche (1989, 1991), Voyiadjis and Kattan (1990, 1991), and Voyiadjis and Sivakumar (1991, 1994) models. The stress rate is incorporated in the evolution equation of the backstress through the addition of a new term. The new term creates an influence of the stress rate on the movement of the yield surface, as proposed by Phillips et al. (1974). This additional term is also dependent on the proximity of the yield surface from the bounding surface and on the length of the chord of the bounding surface in the direction of loading. The evolution equation of the backstress is given as four components of the type NLK-T (Non-Linear Kinematic with Threshold) as proposed by Chaboche (1989). When analyzed for monotonic and cyclic tension loadings on 316 stainless steel, this model was better correlated with the experimental results than the NLK-T model. The proposed model was also tested for non-proportional loading for plastic strain controlled cyclic test with a combined axial force and torque for thin-walled tubular specimens of 60/40 brass. The results obtained were very close to the experimental values by Shiratori et al. (1979). It was also noted that when it was tested for proportional and non-proportional ratcheting, the results were very similar to the

experiments, although the decrease in the strain accumulation does not decrease as fast as in the experimental results.

A finite element continuum mechanics approach is adopted here to study cyclic plasticity. In order to accomplish this objective, a thermodynamic consistent model is developed for the evolution equation of the backstress. This led to a modified model (FAPC model) of the nonlinear Frederick and Armstrong kinematic hardening model with an additional term that allows for the motion of the yield surface to conform well with the experimental observations (see Phillips et al., 1974; Phillips and Weng, 1975) that show the motion of the center of the yield surface in the stress space is directed between the gradient to the surface at the stress point and the stress rate direction at that point. Therefore, the motivation of this work is similar to that of Voyiadjis and Basuroychowdhary (1998) and Basuroychowdhury and Voyiadjis (1998), where the influence of the stress rate on the movement of the yield surface is considered, as proposed by Phillips and his co-workers (1974), Phillips and Weng (1975), Phillips and Lee (1979) and Phillips and Lu (1984). This model is similar in purpose to that of Voyiadjis and Basuroychowdhary (1998) and Basuroychowdhury and Voyiadjis (1998); however, their proposed kinematic hardening rule is rate dependent which is not the case in the model proposed here. The derived isotropic hardening function is similar to the one proposed by Chaboche (1991). The yield criterion, flow rule, and hardening rules are established to ensure that the state of stress always lies on the loading surface. Numerical integration of the incremental elasto-plastic constitutive equations is based on a simple semi-implicit return algorithm (Sivakumar and Voyiadjis, 1997). The full Newton–Raphson iterative method is used to solve the resulting nonlinear equations. The equations of the model are integrated analytically for the case of uniaxial monotonic loading and the associated material parameters are then determined utilizing a nonlinear regression analysis for uniaxial and cyclic proportional loading. The proposed kinematic hardening rule is further modified in order to simulate nonproportional cyclic hardening by using a nonproportionality measure proposed by Voyiadjis and Basuroychowdhary (1998), and Basuroychowdhury and Voyiadjis (1998), which is defined as the angle between the current stress increment and the previous stress increment. This measure represents the topology of the incremental stress path. Experimental simulations are conducted for proportional and non-proportional cyclic loadings. Recently Chun et al. (2002a,b) also used a similar concept defined as the angle between two successive stress vectors.

2. Governing equations of the elasto-plastic model

Since the elasto-plastic response of anisotropic materials is considered here, the hardening in plasticity is introduced as hidden independent internal state variables in the thermodynamic state potential. The Helmoltz free specific energy is considered as the thermodynamic state potential depending on both observable and internal state variables. The form of this potential in terms of the observable variable (T) and internal state variables $\left(\boldsymbol{\varepsilon}^{\mathrm{e}},\ p,\ \boldsymbol{\alpha}^{(k)}\right)$ can be given as:

$$\Psi = \hat{\Psi}\left(\varepsilon^{\mathrm{e}}_{ij}, T, p, \alpha^{(k)}_{ij}\right) \tag{2}$$

where p and $\boldsymbol{\alpha}^{(k)}$ ($k = 1, 2, \ldots, M$) variables characterize the isotropic and kinematic hardening flux variables in plasticity, respectively, and M being the number of desired kinematic hardening components. In Eq. (2) T characterizes the temperature and ε^{e} is the elastic component of the strain tensor where for small strain problems an additive decomposition of the total strain rate can be assumed with ε^{e} being the elastic component and ε^{p} being the corresponding plastic component such that:

$$\dot{\varepsilon}_{ij} = \dot{\varepsilon}^{\mathrm{e}}_{ij} + \dot{\varepsilon}^{\mathrm{p}}_{ij} \tag{3}$$

where the superscripts e and p designate the elastic and plastic components, respectively. Moreover, in this work the subscripted letters after the variables indicate the tensorial nature of the variables unless specifically stated otherwise.

The rate of the isotropic hardening variable of plasticity, $\dot{p}$, is defined as the effective plastic strain and expressed as:

$$\dot{p} = \sqrt{\frac{2}{3}\dot{\varepsilon}^{\mathrm{p}}_{ij}\dot{\varepsilon}^{\mathrm{p}}_{ij}} \tag{4}$$

The time derivative of Eq. (2) with respect to its internal state variables is given by:

$$\dot{\Psi} = \frac{\partial \Psi}{\partial \varepsilon^{\mathrm{e}}_{ij}}\dot{\varepsilon}^{\mathrm{e}}_{ij} + \frac{\partial \Psi}{\partial T}\dot{T} + \frac{\partial \Psi}{\partial p}\dot{p} + \sum_{k=1}^{M}\frac{\partial \Psi}{\partial \alpha^{(k)}_{ij}}\dot{\alpha}^{(k)}_{ij} \tag{5}$$

From the second law of thermodynamics, the Clausius–Duhem inequality is expressed as follows:

$$\sigma_{ij}\dot{\varepsilon}_{ij} - \rho\left(\dot{\Psi} + s\dot{T}\right) - q_i\frac{T_{,i}}{T} \geqslant 0 \tag{6}$$

where $\boldsymbol{\sigma}$ is the Cauchy stress tensor, ρ is the material density, q_i is the heat flux vector, $T_{,i}$ is the temperature gradient, s is the specific entropy per unit mass, and $\dot{\boldsymbol{\varepsilon}}$ is the total strain rate.

Substitution of Eq. (5) into Eq. (6) yields the following expression:

$$\left(\sigma_{ij} - \rho\frac{\partial \Psi}{\partial \varepsilon^{\mathrm{e}}_{ij}}\right)\dot{\varepsilon}^{\mathrm{e}}_{ij} + \sigma_{ij}\dot{\varepsilon}^{\mathrm{p}}_{ij} - \rho\left(\frac{\partial \Psi}{\partial T} + s\right)\dot{T} - \rho\frac{\partial \Psi}{\partial p}\dot{p} - \sum_{k=1}^{M}\rho\frac{\partial \Psi}{\partial \alpha^{(k)}_{ij}}\dot{\alpha}^{(k)}_{ij} - q_i\frac{T_{,i}}{T} \geqslant 0 \tag{7}$$

from which the following thermodynamic state laws are obtained:

$$\sigma_{ij} = \rho\frac{\partial \Psi}{\partial \varepsilon^{\mathrm{e}}_{ij}}; \quad s = -\frac{\partial \Psi}{\partial T}; \quad R = \rho\frac{\partial \Psi}{\partial p}; \quad \text{and} \quad X^{(k)}_{ij} = \rho\frac{\partial \Psi}{\partial \alpha^{(k)}_{ij}} \quad (k = 1, 2 \ldots, M) \tag{8}$$

Eq. (8) describes the relation between the internal state variables and their associated thermodynamic conjugate forces, where $\boldsymbol{\sigma}$, s, R, and $\boldsymbol{X}^{(k)}$ ($k = 1, 2, ..., M$) are the conjugate forces corresponding to the internal state variables $\boldsymbol{\varepsilon}^{\mathrm{e}}$, T, p, and $\boldsymbol{\alpha}^{(k)}$, respectively.

Through this formulation a thermodynamic consistent model suitable for cyclic plasticity of ductile materials is obtained. The internal state variables are selected independently of one another. Moreover, one can assume decoupling between the elastic behavior and hardening, with the specific free energy, Eq. (2), being decomposed into elastic Ψ^{e} and plastic Ψ^{p} parts:

$$\Psi = \Psi^{\mathrm{e}}\left(\varepsilon_{ij}^{\mathrm{e}}, T\right) + \Psi^{\mathrm{p}}\left(p, \alpha_{ij}^{(k)}, T\right) \tag{9}$$

Hence, the Helmholtz free energy Ψ can be expressed in an analytical form of each of its internal state variables as follows:

$$\rho\Psi = \frac{1}{2}\left(\varepsilon_{ij} - \varepsilon_{ij}^{\mathrm{p}}\right)E_{ijkl}\left(\varepsilon_{kl} - \varepsilon_{kl}^{\mathrm{p}}\right) + \frac{1}{3}\sum_{k=1}^{M} C^{(k)}\alpha_{ij}^{(k)}\alpha_{ij}^{(k)} + Q\left(p + \frac{1}{b}\mathrm{e}^{-b\mathrm{p}}\right) \tag{10}$$

where $\boldsymbol{E}$ is the fourth-order elastic stiffness tensor and C, Q and b are material-dependent constants.

The thermodynamic state laws can be obtained from the thermodynamic potential equation, Eq. (10), by making use of Eqs. (8) as shown below:

$$\sigma_{ij} = E_{ijkl}\left(\varepsilon_{kl} - \varepsilon_{kl}^{\mathrm{p}}\right) \tag{11}$$

$$X_{ij}^{(k)} = \frac{2}{3}C^{(k)}\alpha_{ij}^{(k)} \quad (k = 1, 2, \ldots, M) \tag{12}$$

$$R = Q\left(1 - \mathrm{e}^{-b\mathrm{p}}\right) \tag{13}$$

where $\boldsymbol{X}^{(k)}$ ($k = 1, 2, ..., M$) are the variables that describe the movement of the yield surface corresponding to the kinematic hardening, and R is the variable that describes the change in the size of the yield surface corresponding to the isotropic hardening.

It is assumed further that the kinematic hardening conjugate force, $\boldsymbol{X}$, consists of M components as proposed by Chaboche and Rousselier (1981, 1983), where each component is made to evolve independently, such that:

$$X_{ij} = \sum_{k=1}^{M} X_{ij}^{(k)} \tag{14}$$

It follows from Eq. (12) that $\boldsymbol{X}$ can be rewritten as:

$$X_{ij} = \frac{2}{3}\sum_{k=1}^{M} C^{(k)}\alpha_{ij}^{(k)} \tag{15}$$

The Chaboche model has gained popularity and has been implemented into several commercial finite element codes in recent years. This model shows an excellent correlation with the experimental results for monotonic and cyclic loadings (Lemaitre and Chaboche, 1990).

In order to describe the evolution equations of the internal state variables, one needs to define first the plastic dissipation energy, Π, as the sum of the product of the associated variables with the corresponding flux variables in such a way that it can be given by substituting the thermodynamic state laws, Eqs. (8), back into the Clausius–Duhem inequality, Eq. (7):

$$\Pi = \sigma_{ij}\dot{\varepsilon}^{\mathrm{p}}_{ij} - \sum_{k=1}^{M} X^{(k)}_{ij}\dot{\alpha}^{(k)}_{ij} - R\dot{p} \geqslant 0 \tag{16}$$

Using the Legendre–Fenchel transformation of plastic dissipation potential, F, one can obtain the complementary laws in the form of flux variables as function of the dual variables as follows:

$$F = F\left(\sigma_{ij}, X^{(k)}_{ij}, R;\ \varepsilon^{\mathrm{e}}_{ij}, \alpha^{(k)}_{ij}, p\right) \geqslant 0 \tag{17}$$

In this work the evolution equations of the internal state variables are obtained through the use of the generalized normality rule of thermodynamics. In this regard the evolution laws for the plastic strain rate, $\dot{\boldsymbol{\varepsilon}}^{\mathrm{p}}$, the rate of the kinematic hardening flux, $\dot{\boldsymbol{\alpha}}^{(k)}$ $(k = 1, 2, \ldots, M)$, and the rate of the isotropic hardening flux, $\dot{p}$, can be obtained by utilizing the calculus of function of several variables with the Lagrange multiplier, $\dot{\lambda}$, in order to construct the objective function Ω in the following form:

$$\Omega = \Pi - \dot{\lambda}F \tag{18}$$

In order to obtain $\dot{\boldsymbol{\varepsilon}}^{\mathrm{p}}$, $\dot{\boldsymbol{\alpha}}^{(k)}$, and $\dot{p}$, the following conditions are used to maximize the objective function, Ω, respectively:

$$\frac{\partial\Omega}{\partial\sigma_{ij}} = 0, \quad \frac{\partial\Omega}{\partial X^{(k)}_{ij}} = 0 \ \ (k = 1, 2, \ldots, M), \ \text{ and } \quad \frac{\partial\Omega}{\partial R} = 0 \tag{19}$$

By Substituting Eq. (18) into the above relations, the corresponding flow laws of $\dot{\boldsymbol{\varepsilon}}^{\mathrm{p}}$, $\dot{\boldsymbol{\alpha}}^{(k)}$, and $\dot{p}$ are obtained, respectively, as follows:

$$\dot{\varepsilon}^{\mathrm{p}}_{ij} = \dot{\lambda}\frac{\partial F}{\partial\sigma_{ij}}; \quad \dot{\alpha}^{(k)}_{ij} = -\dot{\lambda}\frac{\partial F}{\partial X^{(k)}_{ij}} \quad (k = 1, 2, \ldots, M); \ \text{ and } \quad \dot{p} = -\dot{\lambda}\frac{\partial F}{\partial R} \tag{20}$$

where $\dot{\lambda}$ is the multiplier of time-independent plasticity which will be determined later.

The next important step is the selection of the appropriate form of the dissipation potential, F, in order to establish the desired constitutive equations that describe the mechanical behavior of the material.

3. Plastic dissipation potential and evolution equations

Nonlinear evolution equations for plastic hardening flow rules are required in order to obtain good correlation with the experimental results in cyclic hardening. In order to obtain a nonlinear kinematic hardening rule, the plastic potential function, F, is chosen to be different than the yield function, f. This is achieved by a proper selection of the analytical form of the potential that is defined in Eq. (17). In order to be consistent and satisfy the generalized normality rule of thermodynamics, the following form of the plastic potential function, F, is defined here as follows:

$$F = f + \frac{3}{4}\sum_{k=1}^{M}\frac{\gamma^{(k)}}{C^{(k)}}X_{ij}^{(k)}X_{ij}^{(k)} - \frac{3}{2}\frac{\dot{\sigma}_{ij}}{\dot{p}}\sum_{k=1}^{M}\frac{\beta^{(k)}}{C^{(k)}}X_{ij}^{(k)} \tag{21}$$

where γ and β are constants used to adjust the units of the equation. f is a yield function of a von Mises type defined as follows:

$$f = \sqrt{\frac{3}{2}\left(\tau_{ij} - X_{ij}\right)\left(\tau_{ij} - X_{ij}\right)} - \sigma_{yp} - R(p) \leqslant 0 \tag{22}$$

where σ_{yp} is the initial yield value obtained from simple uniaxial test and $\tau_{ij} = \sigma_{ij} - \frac{1}{3}\sigma_{kk}\delta_{ij}$ is the deviatoric component of the Cauchy stress tensor, $\boldsymbol{\sigma}$. The evolution equations of $\boldsymbol{X}$ and R are derived below.

It is worthy to mention that the second term on the right hand side in Eq. (21) is included in order to retain the Armstrong and Frederick (1966) nonlinear kinematic hardening rule. While the inclusion of the third term is motivated by the experimental observations of Phillips et al. (1974) and Phillips and Weng (1975) that show that the motion of the center of the yield surface in the stress space is directed between the gradient to the surface at the stress point and the stress rate direction at that point.

Introducing Eq. (21) into Eqs. (20) the following expressions are obtained:

$$\dot{\varepsilon}_{ij}^{\mathrm{p}} = \dot{\lambda}\frac{\partial f}{\partial \tau_{ij}} = -\dot{\lambda}\frac{\partial f}{\partial X_{ij}} \tag{23}$$

$$\dot{p} = \dot{\lambda} \tag{24}$$

$$\dot{\alpha}_{ij}^{(k)} = -\dot{\lambda}\left(\frac{\partial f}{\partial X_{ij}^{(k)}} + \frac{3}{2}\frac{\gamma^{(k)}}{C^{(k)}}X_{ij}^{(k)} - \frac{3}{2}\frac{\dot{\sigma}_{ij}}{\dot{p}}\frac{\beta^{(k)}}{C^{(k)}}\right) \tag{25}$$

Substitution of Eqs. (22) and (24) into Eq. (23) give the following expression for the evolution of the plastic strain tensor, $\dot{\boldsymbol{\varepsilon}}^{\mathrm{p}}$:

$$\dot{\varepsilon}_{ij}^{\mathrm{p}} = \frac{3}{2}\left(\frac{\tau_{ij} - X_{ij}}{\sigma_{yp} + R}\right)\dot{p} \tag{26}$$

It can be shown from Eqs. (22) and (23) that the following relation is valid:

$$\dot{\varepsilon}_{ij}^{\mathrm{p}} = -\dot{\lambda}\frac{\partial f}{\partial X_{ij}^{(k)}} \tag{27}$$

Therefore, substitution of Eqs. (24) and (27) into Eq. (25) yields the following expression for the evolution of the k-th kinematic hardening flux variable, such that:

$$\dot{\alpha}_{ij}^{(k)} = \dot{\varepsilon}_{ij}^{p} - \frac{3\gamma^{(k)}}{2C^{(k)}}X_{ij}^{(k)}\dot{p} + \frac{3\beta^{(k)}}{2C^{(k)}}\dot{\sigma}_{ij} \quad (k = 1, 2, \ldots, M) \tag{28}$$

Taking the time derivative of the conjugate forces of Eqs. (11)–(13), and (15) yields the following relations:

$$\dot{\sigma}_{ij} = E_{ijkl}\left(\dot{\varepsilon}_{kl} - \dot{\varepsilon}_{kl}^{\mathrm{p}}\right) \tag{29}$$

$$\dot{X}_{ij}^{(k)} = \frac{2}{3}C^{(k)}\dot{\alpha}_{ij}^{(k)} \quad (k = 1, 2, \ldots, M) \tag{30}$$

$$\dot{R} = bQ\dot{p}\mathrm{e}^{-b\mathrm{p}} \tag{31}$$

$$\dot{X}_{ij} = \frac{2}{3}\sum_{k=1}^{M}C^{(k)}\dot{\alpha}_{ij}^{(k)} \tag{32}$$

By substituting Eq. (28) into Eq. (30), the following evolution equation for the backstress tensor is obtained, such that:

$$\dot{X}_{ij}^{(k)} = \frac{2}{3}C^{(k)}\dot{\varepsilon}_{ij}^{\mathrm{p}} + \beta^{(k)}\dot{\sigma}_{ij} - \gamma^{(k)}X_{ij}^{(k)}\dot{p} \quad (k = 1, 2, \ldots, M) \tag{33}$$

where $C^{(k)}$, $\gamma^{(k)}$, and $\beta^{(k)}$ $(k = 1, 2, \ldots, M)$ are material constants to be calibrated from available experimental data.

Substitution of Eq. (28) into Eq. (32) results in a general expression for the evolution equation of the kinematic hardening rule, such that:

$$\dot{X}_{ij} = \left(\tfrac{2}{3}C\dot{\varepsilon}_{ij}^{\mathrm{p}} + \beta\dot{\sigma}_{ij}\right) - \gamma X_{ij}\dot{p} \tag{34}$$

where

$$C = \sum_{k=1}^{M}C^{(k)},\ \gamma X_{ij} = \sum_{k=1}^{M}\gamma^{(k)}X_{ij}^{(k)},\ \beta = \sum_{k=1}^{M}\beta^{(k)},\ \dot{X}_{ij} = \sum_{k=1}^{M}\dot{X}_{ij}^{(k)} \tag{35}$$

The backstress is then used in conjunction with the bounding surface concept as proposed by Krieg (1975), Dafalias and Popov (1975, 1976), and modified by Voyiadjis and Basuroychowdhury (1998).

The derived kinematic hardening model [Eq. (34)] shows that a new term is generated in the evolution equation of the backstress of the Armstrong and Frederick

model (1966). If $\gamma = \beta = 0$, we retrieve the classical linear kinematic hardening rule (Prager, 1956). If $C = \gamma = 0$, this implies that the movement of the yield surface is along the direction of the stress rate as suggested by Phillips and Weng (1975). If $C \neq 0$, $\beta \neq 0$, and $\gamma = 0$, we obtain the Voyiadjis–Kattan kinematic hardening rule (Voyiadjis and Kattan, 1990, 1991), which shows the motion of the center of the yield surface in the stress space is directed between the gradient to the surface at the stress point and the stress rate direction at that point. This confirms well to the experimental observations by Phillips and his co-workers (1974), Phillips and Weng (1975), Phillips and Lee (1979) and Phillips and Lu (1984). If $\gamma \neq 0$ a nonlinearity is introduced which imposes the introduction of the plastic potential as a modification of the yield function. This allows a good modeling of the cyclic behavior of many metals. Hence, the γ term determines the rate at which the saturation of backstress decreases with increasing plastic strain. In addition, if $C \neq 0$, $\gamma \neq 0$, $\beta = 0$, one obtains the additive decomposition of the backstress into M-components of Fredrick and Armstrong hardening type as proposed by Chaboche and Rousselier (1981, 1983). Motivated by all of those models, the derived kinematic hardening rule is referred to as **FAPC** (Fredrick and Armstrong–Phillips–Chaboche) rule in this paper. All the corresponding kinematic hardening flow rules may be obtained as special cases of the current derived FAPC rule.

In order to derive the evolution of the isotropic hardening function, a relation between R and p can be obtained from Eq. (13), such that:

$$p = -\frac{1}{b}\ln\left(1 - \frac{R}{Q}\right) \tag{36}$$

which upon substituting it into Eq. (31) yields the following expression for $\dot{R}$, such that:

$$\dot{R} = b[Q - R]\dot{p} \tag{37}$$

This expression is similar to the evolution equation proposed by Chaboche (1989, 1991), where it is further proposed that the asymptotic value Q of the isotropic hardening is no longer constant but depends on the memory of deformation (q). In this work the form suggested by Chaboche (1991) will be used, as follows:

$$Q = Q_M + (Q_o - Q_M)\mathrm{e}^{-2\mu q} \tag{38}$$

where Q_M, Q_o, and μ are material constants. The variable q stores one-half of the plastic strain amplitude in each cycle $\left\|\Delta\varepsilon^{\mathrm{p}}/2\right\|$, which in turn depends on the total strain amplitude to which the material is subjected in cyclic loading.

4. The elasto-plastic tangent stiffness

The plastic flow requires that the representative point of the stress state does not leave the yield surface ($f > 0$ is impossible), which is called the consistency condition in plasticity. In order to find the plastic multiplier, $\dot{\lambda}$, the consistency condition ($\dot{f} = 0$) is used, such that:

$$\dot{f} \equiv \frac{\partial f}{\partial \tau_{ij}} \dot{\tau}_{ij} + \sum_{k=1}^{M} \frac{\partial f}{\partial X_{ij}^{(k)}} \dot{X}_{ij}^{(k)} + \frac{\partial f}{\partial R} \dot{R} = 0 \tag{39}$$

However, from the yield function in Eq. (22), it is shown that $\partial f/\partial \boldsymbol{X}^{(k)} = \partial f/\partial \boldsymbol{X}$. Using this result along with Eq. (14), the consistency condition can be written as follows:

$$\dot{f} \equiv \frac{\partial f}{\partial \tau_{ij}} \dot{\tau}_{ij} + \frac{\partial f}{\partial X_{ij}} \dot{X}_{ij} + \frac{\partial f}{\partial R} \dot{R} = 0 \tag{40}$$

Furthermore, the consistency condition may be expressed as follows:

$$\frac{\partial f}{\partial \sigma_{ij}} \left(\dot{\sigma}_{ij} - \dot{X}_{ij} \right) - \dot{R} = 0 \tag{41}$$

Substitution of the evolution equations presented in Eqs. (29), (34), and (37) into Eq. (41) gives the plastic multiplier, $\dot{\lambda}$, as follows:

$$\dot{\lambda} = \left\langle \frac{(1-\beta)}{H} \frac{\partial f}{\partial \sigma_{ij}} E_{ijkl} \dot{\varepsilon}_{kl} \right\rangle \tag{42}$$

where $\langle x \rangle$ denotes the MacAuley bracket defined by $\langle x \rangle = (x + |x|)/2$, which designates the positive part of x, and H is given by

$$H = C + \frac{\partial f}{\partial \sigma_{ij}} E_{ijkl} \frac{\partial f}{\partial \sigma_{kl}} (1-\beta) - \gamma X_{ij} \frac{\partial f}{\partial \sigma_{ij}} + b(Q - R) \tag{43}$$

The elasto-plastic tangent stiffness, $\boldsymbol{D}$, is defined by the rate relation, Eq. (29), such that:

$$\dot{\sigma}_{ij} = E_{ijkl} \left(\dot{\varepsilon}_{kl} - \dot{\varepsilon}_{kl}^{\mathrm{p}} \right) = E_{ijkl} \left(\dot{\varepsilon}_{kl} - \dot{\lambda} \frac{\partial f}{\partial \sigma_{kl}} \right) \tag{44}$$

or

$$\dot{\sigma}_{ij} = D_{ijkl} \dot{\varepsilon}_{kl} \tag{45}$$

where

$$D_{ijkl} = \begin{cases} E_{ijkl} & \text{if } f < 0 \text{ or } \dot{f} < 0 \ \ (\dot{\lambda} = 0, \quad \dot{\lambda} f = 0) \\ E_{ijkl} - \dfrac{(1-\beta)}{H} E_{ijrs} \dfrac{\partial f}{\partial \sigma_{rs}} E_{klmn} \dfrac{\partial f}{\partial \sigma_{mn}} & \text{if } f = 0 \text{ and } \dot{f} = 0 \ \ (\dot{\lambda} > 0, \quad \dot{\lambda} \dot{f} = 0) \end{cases} \tag{46}$$

5. A simple semi-implicit correction algorithm

We will use in this work the Sivakumar and Voyiadjis (1997) semi-implicit scheme in integrating the developed set of nonlinear constitutive equations. This method

corrects implicitly the updated quantities in order to avoid the yield surface drift. No iterations are involved in this scheme. The discrete consistency method is used in the proposed method such that the final state of the yield condition after the end of $(n+1)$th step is given by:

$$f_{n+1}(\tau_{ij}+\Delta\tau_{ij}, X_{ij}+\Delta X_{ij}, R+\Delta R) = f_n(\tau_{ij}, X_{ij}, R) + \Delta f = 0 \tag{47}$$

where the Δ-symbol indicates the difference between the values of a variable at the end of $(n+1)^{\text{th}}$ step and n^{th} step, e.g. $\Delta\boldsymbol{\tau} = \boldsymbol{\tau}_{n+1} - \boldsymbol{\tau}_n$. But since $f_n = 0$, it follows that $\Delta f = 0$. The function Δf contains incremental terms yielding a polynomial equation in $\Delta\lambda$. Hence, given the values obtained in the nth step, the value of $\Delta\lambda$ needed for the drift correction in $(n+1)$th step can be obtained. The advantage of this correction procedure is that all the quantities are corrected simultaneously unlike the stress-correction algorithms where only the stress is corrected due to drift of the yield surface.

Converting the deviatoric stress quantities to normal stress quantities and using the von Mises criterion [Eq. (22)] at $(n+1)$th step along with the consistency condition [Eq. (39)], one can easily show that the final state yield condition [Eq. (47)] becomes:

$$\frac{3}{2}(\Delta\sigma_{ij} - \Delta X_{ij})(\Delta\sigma_{ij} - \Delta X_{ij}) - \frac{1}{2}(\Delta\sigma_{kk})^2 - (\Delta R)^2 = 0 \tag{48}$$

Further substituting the expressions for $\Delta\boldsymbol{\sigma}$, $\Delta\boldsymbol{X}$, and ΔR from Eqs. (29), (34), and (37), respectively, yields the following quadratic polynomial expression in terms of $\Delta\lambda$ with coefficients in terms of the initial values:

$$\bar{a}\Delta\lambda^2 + \bar{b}\Delta\lambda + \bar{c} = 0 \tag{49}$$

where

$$\bar{a} = a_1 l_{ij} l_{ij} - 2a_2 l_{ij}(\gamma X_{ij}) + \frac{4}{3} C a_2 k_{ij} m_{ij} + \frac{4}{9} C^2 m_{ij} m_{ij} - \frac{4}{3} C(\gamma X_{ij}) m_{ij} + (\gamma X_{ij}) \times (\gamma X_{ij}) - \frac{2}{3} r^2 - \frac{1}{3} J_{pp} J_{qq} \tag{50}$$

$$\bar{b} = 2a_2 k_{ij}(\gamma X_{ij}) - 2a_1 l_{ij} k_{ij} - \frac{4}{3} C a_2 k_{ij} m_{ij} + \frac{2}{3} n_{pp} J_{qq} \tag{51}$$

$$\bar{c} = 2a_1 k_{ij} k_{ij} - \frac{1}{3} n_{pp} n_{qq} \tag{52}$$

with $k_{ij} = E_{ijkl}\Delta\varepsilon_{kl}$, $m_{ij} = \partial f/\partial\sigma_{ij}$, $l_{ij} = E_{ijkl} m_{kl}$, $n_{pp} = E_{qqkl}\Delta\varepsilon_{kl}$, $J_{pp} = E_{qqkl} m_{kl}$, $r = b[Q - R]$, $a_1 = 1 - 2\beta + \beta^2$, $a_2 = 1 - \beta$, and $\gamma X_{ij} = \sum_{k=1}^{M} \gamma^{(k)} X_{ij}^{(k)}$.

Solving Eq. (49) yields a positive value and a negative value of $\Delta\lambda$. By taking the positive value and substituting it into Eq. (44), yields the updated value of the stress increment.

6. Identification of the material constants

Identification of the material constants associated with any proposed material model is one of the most challenging issues for researchers in order to obtain better representation of their material models. The identification procedure for the material constants involved in the described backstress evolution equation is based on available experimental results. If limited test data are available, C, γ, and β can be based on the stress-strain data obtained from the half cycle of the uniaxial tension or compression experiments. Example of such test data is shown in Fig. 1. This approach is usually adequate when the simulation involves only a few cycles of loading. The details of the procedure to determine the material constants are outlined below. Although it may be lengthy, it is important to describe such procedures for elaborate constitutive models.

Integration of the backstress evolution law, Eq. (34), over a half cycle of the stress–strain data (Fig. 1) can be performed by assuming that for each data point (σ_i, $\varepsilon_i^{\mathrm{p}}$) a value of X is obtained such that:

$$X = \sigma - \left(\sigma_{yp} + R\right) \tag{53}$$

From which the stress rate can be expressed as follows:

$$\dot{\sigma} = \dot{X} + \dot{R} \tag{54}$$

For uniaxial tension or compression loading and more generally, in proportional loading, if the plastic strain increment in the direction of loading is $\dot{\varepsilon}^{\mathrm{p}}$ ($\dot{\varepsilon}_{11}^{\mathrm{p}} = \dot{\varepsilon}^{\mathrm{p}}$) and since the plastic straining is assumed to be incompressible (Poisson's ratio is effectively 0.5), then from Eq. (2) the effective plastic strain rate, $\dot{p}$, becomes:

$$\dot{p} = \sqrt{\tfrac{2}{3}\dot{\varepsilon}_{ij}^{\mathrm{p}}\dot{\varepsilon}_{ij}^{\mathrm{p}}} = \dot{\varepsilon}^{\mathrm{p}} \tag{55}$$

Utilizing Eqs. (54) and (55), Eq. (34) can be rewritten as follows:

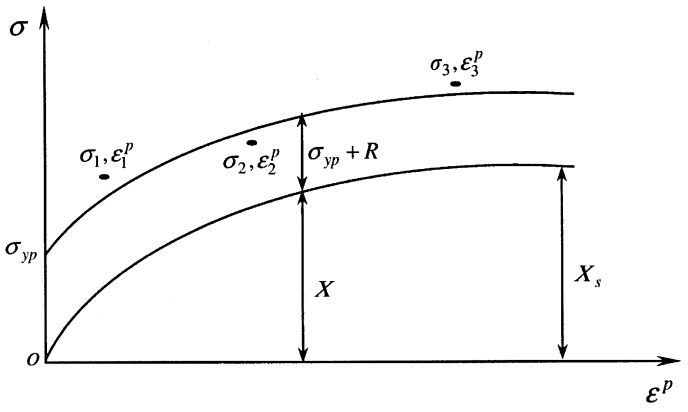

Fig. 1. Half cycle of stress–strain data representing the hardening in the nonlinear kinematic model (● represents experimental data at three different stress levels).

$$dX = \tfrac{2}{3} C\, d\varepsilon^{p} + \beta\, dX + \beta\, dR - \gamma X\, d\varepsilon^{p} \tag{56}$$

Integrating the above expression over a half cycle of the stress strain data at constant R (i.e. assuming translation of the yield surface without change in its size), yields the following expression:

$$X = \frac{2C}{3\gamma} + \left(X_o - \frac{2C}{3\gamma}\right)\exp\left(\frac{-\gamma}{1-\beta}\left(\varepsilon^{p} - \varepsilon_o^{p}\right)\right) \tag{57}$$

and the state (ε_o^{p}, X_o) results from the previous flow.

Using a finite set of points in the uniaxial backstress–plastic strain curve (Fig. 1) one can approximate the curve in the form of Eq. (57). One now calculates C, γ, and β so that the curve passes through the data such that the sum of squares of the vertical differences between the curve and the various data points is minimized (i.e. by using the least-squares error approach). Eq. (57) is not directly amenable to a least-squares error fit because the equation is not that of a straight line. However, the equation is re-arranged in the following form:

$$\ln\left(\frac{2C/3\gamma - X_o}{2C/3\gamma - X}\right) = \frac{\gamma}{1-\beta}\exp\left(\varepsilon^{p} - \varepsilon_o^{p}\right) \tag{58}$$

With known values of $2C/3\gamma$ the least-squares error fit can be used to fit Eq. (58). Close to the saturation point of the stress, X_s (Fig. 1), the hardening (kinematic and isotropic) increment tends to zero. Thus, by substituting $dX = 0$ into Eq. (56), X is reduced to:

$$X_s = \frac{2C}{3\gamma} \tag{59}$$

hence, Eq. (58) can be rewritten as:

$$\ln\left(\frac{X_s - X_o}{X_s - X}\right) = \frac{\gamma}{1-\beta}\exp\left(\varepsilon^{p} - \varepsilon_o^{p}\right) \tag{60}$$

Note that Eq. (60) is of the form

$$y = ax \quad \text{with} \quad y = \ln\left(\frac{X_s - X_o}{X_s - X}\right), \quad a = \frac{\gamma}{1-\beta}, \quad \text{and} \quad x = \exp\left(\varepsilon^{p} - \varepsilon_o^{p}\right) \tag{61}$$

which is the equation of a straight line. That is, one performs a linearizing transformation. Thus, one can now apply a least-squares fit of the transformed variables in the forgoing form. It may be remarked that here it is not necessary to use a process of updating the variables ε_o^{p} and X_o. The state (ε_o^{p}, X_o) results from the previous flow, with the flow always expressed by the same evolutionary equation.

The value of a for a least-squares fit is given by:

$$a = \frac{n\sum(\mathrm{xy}) - \left(\sum x\right)\left(\sum y\right)}{n\sum(x) - \left(\sum x\right)^2} \tag{62}$$

where n is the number of data points and

$$\sum x = \sum_{i=1}^{n} x_i, \quad \sum\left(x^2\right) = \sum_{i=1}^{n}(x_i)^2, \quad \text{and} \quad \left(\sum x\right)^2 = \left(\sum_{i=1}^{n} x_i\right)^2 \tag{63}$$

One now obtains C and γ from Eqs. (59) and $(61)_3$ as follows:

$$C = \frac{3}{2} X_s a(1-\beta) \ \text{ and } \ \gamma = a(1-\beta) \tag{64}$$

However, one has not yet determined the value of β corresponding to a least-squares error fit. Actually, one has obtained only a least-squares fit of C and γ for a specified value of β. To determine β, one needs to minimize the squares of the errors

$$\mathrm{e}^2 = \sum_{i=1}^{n}\left[\bar{X} - X\right]^2 \tag{65}$$

where $\bar{X}$ is the backstress value from the actual data at the n data points, and X is the backstress value from Eq. (57). One does not perform this minimization by finding where the derivative of the error squared is zero. Instead, one searchs for a value of β for which the error is smallest. That is, β is increased in increments from its possible smallest value to the first data point until the error, which first decreases, begins to increase. One, then, successively halves the increment size and searches the region around the minimum until the value of β is found to a desired level of accuracy. It is clear from Eq. (46) that $\beta = \sum_{k=1}^{M}\beta^{(k)} \ll 1$; otherwise the elastic–plastic tangent modulus will be greater than the initial elastic modulus, which is not true. This constraint minimizes the computational cost in finding the converged value of $\beta^{(k)}$.

Similarly, for cyclic loading the relation between the stress amplitude and the plastic strain amplitude can be obtained from the stabilized full cycle of a specimen subjected to symmetrical cycles. Such a stabilized cycle is shown in Fig. 2. Each data pair $(\sigma_i, \ \varepsilon_i^{\mathrm{p}})$ must then be specified with the strain axis shifted to $\varepsilon_o^{\mathrm{p}}$. Integrating the derived backstress evolution equation, Eq. (34), over this uniaxial strain cycle, provides a similar expression as presented previously by Eq. (57). Therefore, the above described procedure used to calibrate the material constants C, γ, and β for uniaxial half-cycle can also be used to obtain the material constants corresponding to the obtained uniaxial stabilized full-cycle data.

It is noteworthy to mention that the uniqueness of the above described procedure for half-cycle and full-cycle of the stress–strain test data (Figs. 1 and 2) is restricted to materials that exhibit high saturation levels of hardening at high stresses for which excellent fittings can be obtained, while it gives relatively poor fitting for materials that exhibit low saturation levels of hardening (i.e. for brittle-like behavior).

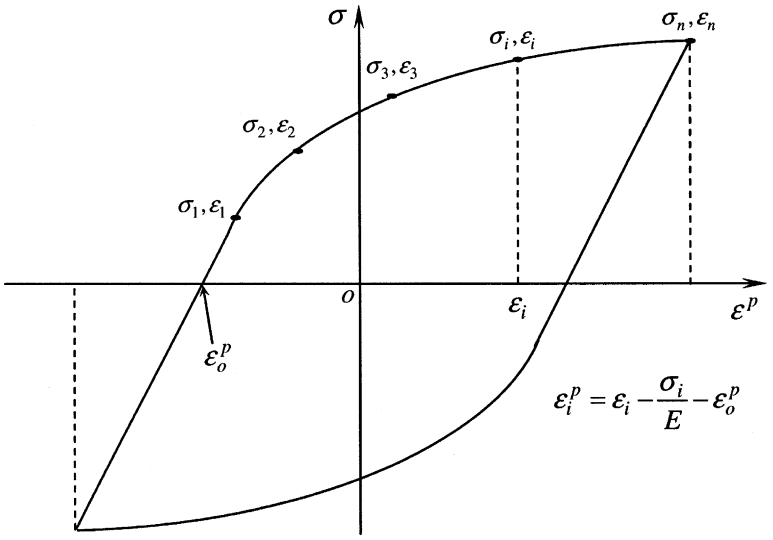

Fig. 2. Stabilized full-cycle of symmetrical uniaxial tensile stress-strain data representing the hardening in the nonlinear kinematic hardening model.

7. Results from simulation of experiments

7.1. Monotonic tensile loading

The proposed model's material constants (C, γ, and β) are determined for 316 stainless steel at room temperature by using the uniaxial monotonic experimental data given by Chaboche (1989, 1991) as shown in Fig. 3. Four kinematic variables ($M=4$) are amply sufficient to obtain the experimental stress–strain curve. Each set of the constants $C^{(k)}$ and $\gamma^{(k)}$ ($k=1, 2, 3$) is obtained using the initial 1.25% strain-range, where $\beta^{(k)}$ ($k=1-4$) constants are set to a 0.15 value. The values of $C^{(k)}$ and $\gamma^{(k)}$ ($k=4$) are determined for the later part of the strain-range beyond 1.25 percent strain. Utilizing the qualitative nature of the parameters $C^{(k)}$ and $\gamma^{(k)}$ observed in uniaxial loading cases, the values of $C^{(k)}$ calibrated using the identification procedure described in Section 6 are further modified to fit the stress–strain uniaxial monotonic response. The general guideline followed is that the decomposed rules ($k=1, 2, 3$) should have high values of C_1, C_2, and C_3 with relatively large values of γ_1, γ_2, and γ_3 to represent the initial high rate of hardening and the smooth nonlinear transitional region. C_4 and γ_4, on the other hand, should have moderate values to represent the mild hardening portion that occurs beyond 1.25 percent strain. The obtained material constants are listed in Table 1. The material constants associated with the isotropic hardening function [Eqs. (37) and (38)] are based on the total range of strain and are taken exactly as reported by Chaboche (1991). Fig. 3 shows the superposition of the different calibrated kinematic hardening and isotropic hardening functions resulting in the fitted stress–plastic strain curve as compared to the corresponding experimental data.

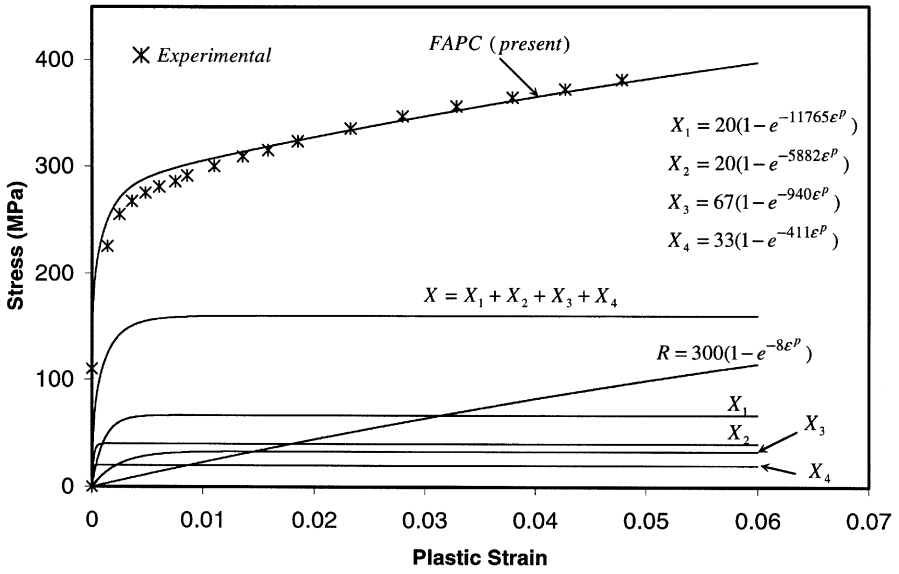

Fig. 3. Superposition of several kinematic hardening models under uniaxial tensile loading for 316L stainless steel ($M = 4$).

Table 1
316 stainless steel material parameters using FAPC proposed model (uniaxial monotonic tensile loading)

$C_1 = 300{,}000$ MPa	$\gamma_1 = 10{,}000$	$\beta_1 = 0.15$	$Q_o = 14$ MPa
$C_2 = 300{,}000$ MPa	$\gamma_2 = 5000$	$\beta_2 = 0.15$	$Q_M = 300$ MPa
$C_3 = 80{,}000$ MPa	$\gamma_4 = 800$	$\beta_3 = 0.15$	$\mu = 10$
$C_4 = 17{,}500$ MPa	$\gamma_4 = 350$	$\beta_4 = 0.15$	$b = 8$
$E = 187{,}000$ MPa	$\sigma_{yp} = 122.5$ MPa	$\nu = 0.30$	

As pointed out previously in Section 6, there is a constraint on the value of β ($\beta \ll 1$). In the current case, decomposition of the backstress into four kinematic variables showed that any arbitrary value for $\beta = \sum_{k=1}^{4} \beta^{(k)}$ must fall between 0.05 and 0.6 (i.e. the upper bound is 0.15 for $\beta^{(k)}$), which gives fair correlation with experimental data but with different identified values of C and γ. During the calibration process, it was noted that any small variation in β has a significant effect on the values of C and γ.

The current material model is implemented in the in-house finite element code **DNA** (Voyiadjis and Kattan, 1999; Kattan and Voyiadjis, 2001). Numerical integration of the incremental elasto-plastic constitutive equations is based on the implicit return-mapping algorithm described in Section 5. The full Newton–Raphson iterative method is used to solve the resulting nonlinear equations. The developed finite element code is used to simulate the available test results obtained by Chaboche (1991) for uniaxial monotonic tensile loading on 316L stainless steel dogbone specimen using the calibrated material constants listed in Table 1. The specimen is analyzed as an axisymmetric problem subjected to a tensile loading at

the free end. Moreover, the stainless steel bar is of diameter 36 mm and gage-length of 60 mm. This problem is classical and has been mostly considered in the literature.

Fig. 4 shows numerical comparisons of the proposed material model (FAPC), Basuroychowdhury and Voyiadjis (1998) model, and Chaboche (1991) model with the corresponding experimental results. The comparisons show better agreement of the FAPC model predictions with the experimental data than the Chaboche model, and the Basuroychowdhury and Voyiadjis model predictions for the case of uniaxial monotonic loading. It is also clear that the proposed model captures the nonlinear hardening behavior and the smooth transition from elastic to plastic deformation relatively better than the Chaboche (1991), and the Basuroychowdhury and Voyiadjis (1998) models. Thus, it is obvious that introducing the β term in the Fredrick and Armstrong evolution equation has a significant effect with regard to the experimental simulations.

7.2. Uniaxial tension–compression cyclic loading

One now calibrates the material constants C, γ, and β for the case of uniaxial tension-compression cyclic loading as proposed in Fig. 2 from a stabilized strain or stress cycle. The stabilized hysteresis loop of the experimental results (Lemaitre and Chaboche, 1990) for the symmetrical stress cycles of 316L stainless steel at room temperature with controlled stress are used here to identify the current material constants. The obtained material constants are slightly different than those obtained in the uniaxial monotonic tensile loading and are listed in Table 2. The difference is only in the C and γ constants.

The material response in a stress-controlled environment is obtained using the developed finite element code (DNA). The uniaxial stress is made to oscillate

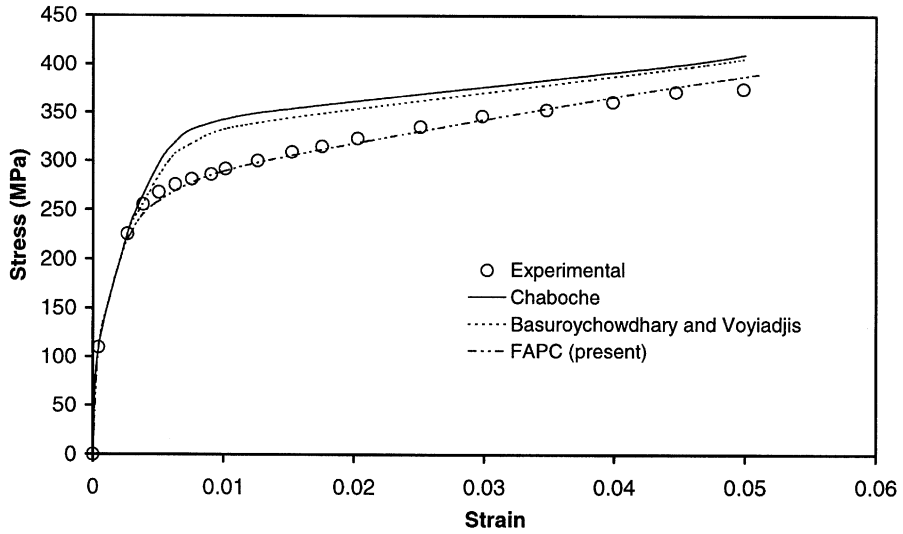

Fig. 4. Finite Element Simulations of uniaxial tensile loading for 316L stainless steel.

Table 2
316 stainless steel material parameters using FAPC proposed model (uniaxial stress-controlled cyclic loading)

$C_1 = 300{,}000$ MPa	$\gamma_1 = 9000$	$\beta_1 = 0.15$	$Q_o = 14$ MPa
$C_2 = 80{,}000$ MPa	$\gamma_2 = 1000$	$\beta_2 = 0.15$	$Q_M = 300$ MPa
$C_3 = 15{,}500$ MPa	$\gamma_4 = 300$	$\beta_3 = 0.15$	$\mu = 10$
$C_4 = 1{,}700$ MPa	$\gamma_4 = 560$	$\beta_4 = 0.15$	$b = 8$
$E = 187{,}000$ MPa	$\sigma_{yp} = 122.5$ MPa	$\nu = 0.30$	

between ± 336 MPa and the corresponding response is plotted in Fig. 5(a). Comparison with the experimental results using the data of the stabilized cycle is given in Fig. 5(b). The response of the model is stabilized after a single cycle which conforms well with the experimental observations in the case of symmetrical cyclic loading (zero-mean stress or no ratcheting).

7.3. Nonproportional cyclic hardening

One now examines the proposed model in order to simulate hardening behavior under nonproportional cyclic loading. Materials such as annealed 304 and 316 stainless steel harden much more under nonproportional cyclic loading than under proportional loading (Lamba and Sidebottom, 1978). A measure representing the degree of nonproportionality of loading is thus necessary. Most of the constitutive models developed for proportional loading failed to predict the nonproportional cyclic hardening as examined by Ohno (1990, 1997). Nonproportionality measures have been proposed in several works (e.g. Benallal and Marquis, 1987; Krempl and Yao, 1987; McDowell, 1985a,b; Tanaka et al., 1987; Krempl and Lu, 1989; Ellyin and Xia, 1989; Chaboche, 1991; Voyiadjis and Sivakumar, 1991, 1994; Ohno and Wang, 1993a, b, 1994; Voyiadjis and Basuroychowdhary, 1998; Basuroychowdhury and Voyiadjis, 1998; Abdel and Ohno, 2000, etc.).

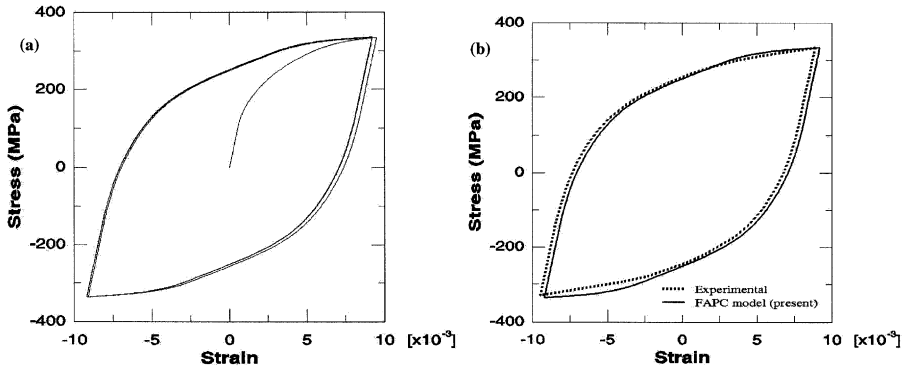

Fig. 5. Cyclic hardening under uniaxial stress-controlled cyclic loading of 316L stainless steel at room temperature: (a) numerical simulation, (b) identification of the stabilized cycle.

However, in this work use is made of the nonproportionality measure introduced by Voyiadjis and Basuroychowdhary (1998), and Basuroychowdhury and Voyiadjis (1998). This measure represents the topology of the incremental stress path. Numerically, it represents the angle between the current stress increment and the previous stress increment (see Fig. 6), such that:

$$\cos\theta = l^{\mathrm{p}}_{ij} l^{\mathrm{c}}_{ij} \tag{66}$$

θ is interpreted numerically using finite stress increments. However, as the stress increment goes to zero, θ is interpreted as the curvature of the stress path (Voyiadjis and Basuroychowdhary, 1998). $\boldsymbol{l}^{\mathrm{c}}$ and $\boldsymbol{l}^{\mathrm{p}}$ are the unit directional tensors for the current stress increment and its corresponding unit directional tensor for the previous increment of stress, respectively, and defined as follows:

$$l^{\alpha}_{ij} = \frac{\dot{\sigma}^{\alpha}_{ij}}{\left\|\dot{\sigma}^{\alpha}_{mn}\right\|} \tag{67}$$

where $\alpha = c$ or p. The superscripts c and p do not imply tensorial indices but merely designate the corresponding stress increment step, where c is for the current stress increment and p is for the previous stress increment.

This measure is introduced here through the material constants $\bar{C}^{(k)}$, $\bar{\beta}^{(k)}$, and $\bar{\gamma}^{(k)}$ ($k = 1, 2, \ldots, M$) associated with the proposed kinematic hardening evolution equation, Eq. (33), to account for the dependence not only on the stress path loading direction but also on the rate of change of the stress path direction, such that:

$$\bar{C}^{(k)} = C^{(k)}\left(1 + \sin^2\theta\right) \quad (k = 1, 2, \ldots, M) \tag{68}$$

$$\bar{\beta}^{(k)} = \beta^{(k)}\left(1 + \sin^2\theta\right) \quad (k = 1, 2, \ldots, M) \tag{69}$$

and

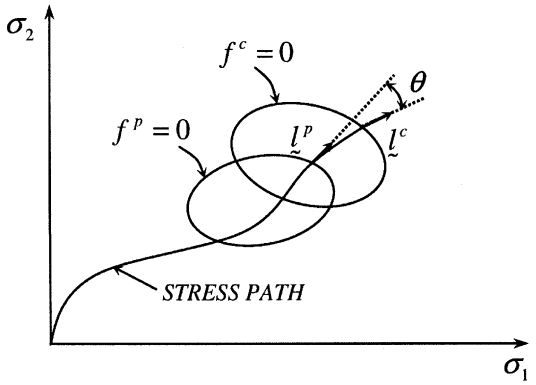

Fig. 6. Schematic representation of the nonproportionality measure (θ).

$$\bar{\gamma}^{(k)} = \gamma^{(k)}\left(1 - \sin^2\theta\right) = \gamma^{(k)}\cos^2\theta \quad (k = 1, 2, \ldots, M) \tag{70}$$

The motivation in postulating such expressions is that the constitutive models that include dynamic recovery terms predict excessive ratcheting (Ohno, 1990, 1997). This is mainly attributed to that the dynamic recovery is too active in those models to simulate ratcheting appropriately. On the other hand, Eqs. (68)–(70) increase the strain hardening terms [first and second terms in Eq. (33)] accompanied by decrease in the dynamic recovery term [the last term in Eq. (33)] as a function of the stress path. It is noteworthy also to mention that the dynamic recovery term operates at all times. This makes the proposed model a nonlinear kinematic hardening model based on strain hardening and dynamic recovery, which is physically sound and numerically attractive.

From Eqs. (68)–(70) one can rewrite the modified backstress evolution expression for $\boldsymbol{X}$ from Eq. (33) as follows:

$$\dot{\bar{X}}_{ij}^{(k)} = \frac{2}{3}\bar{C}^{(k)}\dot{\varepsilon}_{ij}^{\mathrm{p}} + \bar{\beta}^{(k)}\dot{\sigma}_{ij} - \bar{\gamma}^{(k)}\bar{X}_{ij}^{(k)}\dot{p} \quad (k = 1, 2, \ldots, M) \tag{71}$$

In the work of Voyiadjis and Basuroychowdhary (1998), and Basuroychowdhury and Voyiadjis (1998), only $\bar{\beta}^{(k)}$ $(k = 1, 2, \ldots, M)$ and $\bar{C}^{(3)}$ are assumed to be dependent on the nonproportionality measure θ. Different equations are also adapted in their work. However, similar arguments are used here, where it is clear from Eq. (66) that if one considers straight-line stress paths (e.g. uniaxial monotonic loading), the angle θ is zero between the respective stress increment directions and by which one retrieves Eq. (33), which includes only the influence of stress rate direction.

One now utilizes the multiaxial cyclic tests by Tanaka et al. (1985, 1987), which were performed on 316 stainless steel thin-walled tubular specimens at room temperature, in order to verify the applicability of the proposed model in simulating the nonproportional cyclic hardening. The types of tests conducted are shown in Fig. 7. Six types of cyclic loadings are studied here namely, Tension–Compression [Fig. 7(a)], Torsion [Fig. 7(b)], Cruciform I [Fig. 7(c)], Cruciform II [Fig. 7(d)], Square [Fig. 7(e)], and Circular [Fig. 7(f)]. The strain and stress states are represented in terms of the plastic strain vector $\underline{\varepsilon}^{p}$ and the corresponding stress vector $\underline{\sigma}$ in the plastic strain space $(\varepsilon_{11}^{p},\ 2\varepsilon_{12}^{p}/\sqrt{3})$ and the deviatoric stress space $(\sigma_{11}, \sqrt{3}\sigma_{12})$, respectively, and given as follows:

$$\underline{\varepsilon}^{\mathrm{p}} = \varepsilon_{11}^{\mathrm{p}}\underline{n}_1 + 2\varepsilon_{12}^{\mathrm{p}}\underline{n}_2 \tag{72}$$

$$\underline{\sigma} = \sigma_{11}\underline{n}_1 + \sqrt{3}\sigma_{12}\underline{n}_2 \tag{73}$$

where $\underline{n}_1$ and $\underline{n}_2$ designate a set of orthogonal base vectors in the deviatoric space, and $\varepsilon_{11}^{\mathrm{p}}$, $\varepsilon_{12}^{\mathrm{p}}$, σ_{11}, and σ_{12} are the axial plastic strain, the torsional plastic strain, the axial stress, and the torsional stress, respectively. The magnitudes of $\underline{\varepsilon}^{\mathrm{p}}$ and $\underline{\sigma}$ correspond to the effective plastic strain and the equivalent von Mises stress, respectively. The length of the plastic strain path p corresponds to the accumulative or effective plastic strain and is defined as:

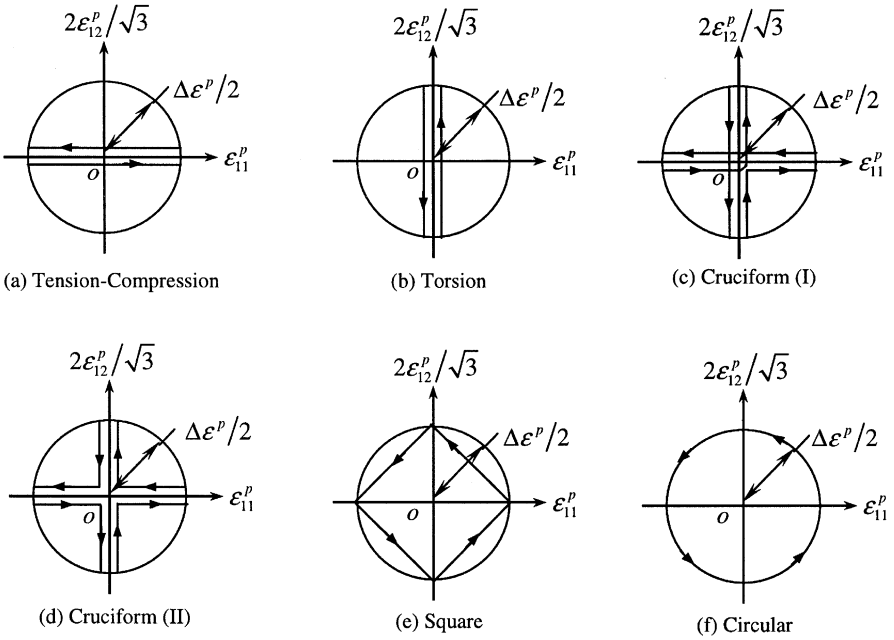

Fig. 7. Cyclic plastic strain paths with $\Delta\varepsilon^p/2 = 0.2\%$ and a constant plastic strain rate $\dot{p} = 3 \times 10^{-5}$/s (Tanaka et al., 1985).

$$p = \int_o^t \left\| \dot{\underline{\varepsilon}}^{\mathrm{p}} \right\| \mathrm{d}t \tag{74}$$

The 316 stainless steel thin-walled tubular specimens were again analyzed using the developed finite element code DNA. The numerical simulations were carried out at room temperature by applying the six representative strain paths in the plastic strain space (i.e. plastic strain controlled cyclic tests) as shown in Fig. 7. A constant equivalent plastic amplitude $\Delta\varepsilon^{\mathrm{p}}/2 = 0.2\%$ and a constant plastic strain rate $\dot{p} = 3 \times 10^{-5}$/s are prescribed for these cyclic tests.

The six fundamental cyclic plastic strain paths shown in Fig. 7 are simulated numerically as shown in Fig. 8 using the developed model, referred to here as FAPC model, and compared with the experimental results obtained by Tanaka et al. (1985). The thin-walled tubular specimens are of outside diameter 21 mm, thickness 1 mm, and gage-length of 60 mm. The material constants used for 316 stainless steel are outlined in Table 2. However, a different Young's modulus than the one given in Table 2 is used to conduct the experimental simulations. Tanaka et al. (1985) evaluated the Young's modulus experimentally, where $E = 203$ GPa as reported in their paper. Moreover, using the FEM the plastic strain path is discretized into sufficient small increments which give saturated measure of the non-proportionality; i.e. the

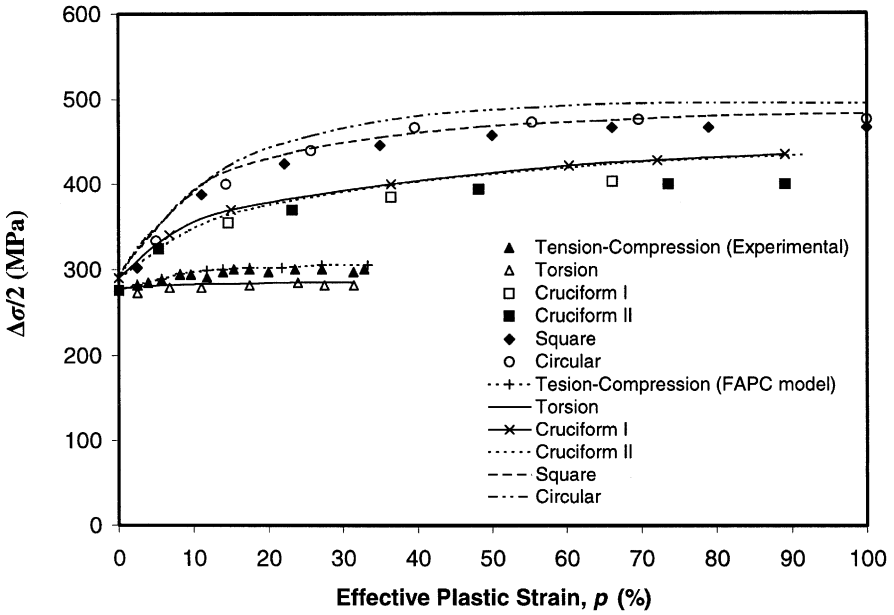

Fig. 8. Effect of cyclic plastic strain paths on cyclic hardening of 316 stainless steel ($\Delta\varepsilon^p/2 = 0.2\%$, $\dot{p} = 3 \times 10^{-5}$/s).

loading increments are chosen so that the non-proportionality measure θ has little influence on the results. Therefore, it is noteworthy to say that if the loading increment is assumed very small, the accuracy in describing the stress or strain paths increases which is advantageous in simulating the nonproportional cyclic hardening. The accuracy in describing the loading path depends on the amount of the load increment and thus the nonproportionality measure θ also depends on the increment size. However, if an analytical solution is sought then the non-proportionality measure θ is interpreted as the curvature of the stress path. A mathematical form of this measure has been proposed by Basuroychowdhury and Voyiadjis (1998). Good correlation between the numerical and experimental results is obtained as indicated in Fig. 8. This proves that the developed model is successful in predicting the dependence of cyclic hardening on the shape of the plastic strain path. In addition, this shows that the proposed non-proportionality measure is appropriate to simulate plastic strain paths consisting of linear branches passing through the origin in the plastic strain space [Fig. 7(a)–(d)] as well as nonlinear continuous plastic strain paths [Fig. 7(f)], where many suggested nonproportionality measures incorporated in several kinematic hardening models failed to do so (Ohno, 1990, 1997). However, the decrease in the stress amplitude does not die down as rapidly as in the experimental results indicated in Fig. 8.

8. Conclusions

A consistent thermodynamic formulation is used in this work in order to derive the present constitutive material model. The derived kinematic hardening rule, which is referred in this paper as **FAPC** (Fredrick and Armstrong–Phillips–Chaboche) rule, is a combination of the Frederick and Armstrong backstress evolution equation (Armstrong and Frederick, 1966), Phillips evolution equation (Phillips et al., 1974), and Chaboche series approach (Chaboche and Rousselier, 1983). All these kinematic hardening rules can be obtained as special cases of the current derived rule. A new term is generated in the Frederick and Armstrong evolution equation in order to incorporate the influence of the stress rate direction on the cyclic hardening. This new kinematic hardening rule is incorporated in a material constitutive model based on the von Mises plasticity type and the Chaboche isotropic hardening type.

The proposed material model has been implemented in the in-house finite element code **DNA** (Voyiadjis and Kattan, 1999; Kattan and Voyiadjis, 2001). The implementation employs a simple implicit return-mapping algorithm proposed by Sivakumar and Voyiadjis (1997) in order to numerically integrate the incremental elasto-plastic constitutive equations. The full Newton–Raphson iterative method is used to solve the resulting nonlinear equations. In addition, the equations of the model are integrated analytically for the case of uniaxial monotonic loading and the associated material parameters are then determined utilizing a nonlinear regression analysis for uniaxial and cyclic proportional loadings. However, the calibrated values of $C^{(k)}$ ($k = 1, 2, ..., M$) are further modified utilizing the qualitative nature of the parameters $C^{(k)}$ and $\gamma^{(k)}$ observed in uniaxial loading cases. Experimental simulations are then conducted using the developed finite element for the case of uniaxial monotonic loading and cyclic proportional loading. Those simulations show that the proposed model captures the nonlinear hardening behavior and the smooth transition from elastic to plastic deformation relatively well.

The model is further modified in order to simulate nonproportional cyclic hardening by using a nonproportionality measure proposed by Voyiadjis and Basuroychowdhary (1998), and Basuroychowdhury and Voyiadjis (1998). This measure accounts for the topology of the incremental stress path. Numerically, it represents the angle between the current stress increment and the previous stress increment. This angle is interpreted numerically using finite stress increments and for very small stress increments. It is interpreted as the curvature of the stress path. This measure has been shown to be successful in predicting the dependence of cyclic hardening on the shape of the plastic strain path. The proposed model is tested for non-proportional loading (multiaxial ratcheting) by obtaining numerical results for a series of cyclic plastic strain paths and comparing it with the experimental results by Tanaka et al. (1985), which are performed on 316 stainless steel thin-walled tubular specimens at room temperature. This shows that the proposed model is quite successful in simulating both the plastic strain paths consisting of linear branches passing through the origin in the plastic strain space as well as for nonlinear continuous plastic strain paths. However, the decrease in the stress amplitude does not die down as rapidly as in the experimental results.

References

Armstrong, P.J., Frederick, C.O., 1966. A Mathematical Representation of the Multiaxial Bauschinger Effect (CEGB Report RD/B/N/731). Berkeley Laboratories, R&D Department, CA.

Abdel, K.M., Ohno, N., 2000. Kinematic hardening model suitable for ratcheting with steady state. International Journal of Plasticity 16, 225–240.

Benallal, A., Marquis, D., 1987. Constitutive equations for nonproportional cyclic elasto-viscoplasticity. ASME J. Eng. Mat. Tech. 109, 326–336.

Basuroychowdhury, I.N., Voyiadjis, G.Z., 1998. A multiaxial cyclic plasticity model for non-proportional loading cases. International Journal of Plasticity 14 (9), 855–870.

Bari, S., Hassan, T., 2002. An advancement in cyclic plasticity modeling for multiaxial ratcheting simulation. International Journal of Plasticity 18, 873–894.

Chaboche, J.-L., Rousselier, G., 1981. On the plastic and viscoplastic constitutive equations based on the internal variables concept. In: SMIRT-6 Post Conf., Paris, T.P. ONERA no. 8-11.

Chaboche, J.-L., Rousselier, G., 1983. On the plastic and viscoplastic constitutive equations, part I: rules developed with internal variable concept. Part II: application of internal variable concepts to the 316 stainless steel. ASME J. Pressure Vessel Tech. 105, 153–164.

Chaboche, J.-L., 1986. Time independent constitutive theories for cyclic plasticity. International Journal of Plasticity 2, 149–188.

Chaboche, J.-L., 1989. Constitutive equations for cyclic plasticity and cyclic viscoplasticity. International Journal of Plasticity 5, 247–302.

Chaboche, J.-L., 1991. On some modifications of kinematic hardening to improve the description of ratcheting effects. International Journal of Plasticity 7, 661–678.

Chun, B.K., Kim, H.Y., Lee, J.K., 2002a. Modeling the Bauschinger effect for sheet metals, part I: theory. International Journal of Plasticity 18, 597–616.

Chun, B.K., Kim, H.Y., Lee, J.K., 2000b. Modeling the Bauschinger effect for sheet metals, part II: applications. International Journal of Plasticity 18, 597–616.

Dafalias, Y.F., Popov, T.T., 1975. A model of nonlinearly hardening materials for complex loading. Acta Mechanica 21, 173–192.

Dafalias, Y.F., Popov, T.T., 1976. Plastic internal variables formulism in cyclic plasticity. Journal of Applied Mechanics, ASME 43, 645–651.

Duszek, K., Perzyna, P., 1991. On combined isotropic and kinematic hardening effects in plastic flow processes. International Journal of Plasticity 7, 351–363.

Dornowski, W., Perzyna, P., 1999. Constitutive modeling of inelastic solids for plastic flow processes under cyclic dynamic loadings. Transactions of ASME, J. Eng. Materials and Technology 121, 210–220.

Dornowski, W., Perzyna, P., 2000. Localization phenomena in thermo-viscoplastic flow processes under cyclic dynamic loadings. Computer Assisted Mechanics and Engineering Sciences 7, 117–160.

Eisenberg, M.A., Phillips, A., 1968. On nonlinear kinematic hardening. Acta Mechanica 5, 1–13.

Ellyin, F., Xia, Z., 1989. A rate-independent constitutive model for transient non-proportional loading. J. Mech. Phys. Solids 37, 71–91.

Geng, L., Wagoner, R.H., 2000. Springback analysis with a modified nonlinear hardening model (SAE2000-01-0410).

Hill, R., 1950. The Mathematical Theory of Plasticity. Oxford, 1950.

Jiang, Y., Kurath, P., 1996. Characteristics of Armstrong-Frederick type plasticity model. International Journal of Plasticity 12, 387–415.

Krieg, R.D., 1975. A practical two surface plasticity theory. Journal of Applied Mechanics, ASME E42, 641–646.

Krempl, E., Yao, D., 1987. The viscoplasticity theory based on overstress applied to ratcheting and cyclic hardening. In: Rie, K.T. (Ed.), Low-Cycle Fatigue and Elasto-Plastic Behavior of Materials. Elsevier, London, pp. 137–148.

Krempl, E., Lu, H., 1989. The path and amplitude dependence of cyclic hardening of type 304 stainless steel at room temperature. In: Brown, M.W., Miller, K.J. (Eds.), Biaxial and Multiaxial Fatigue. Mechanical Engineering Publications, London, pp. 89–106.

Kattan, P.I., Voyiadjis, G.Z., 2001. Damage Mechanics with Finite Elements: Practical Applications with Composite Tools. Springer.

Lemaitre, J., Chaboche, J.-L., 1990. Mechanics of Solid Materials. Cambridge University Press, Cambridge, UK. pp. 212–240.

Lamba, H.S., Sidebottom, O.M., 1978. Cyclic plasticity for nonproportional paths. ASME J. Eng. Mat. Tech. 100, 96–111.

Mroz, Z., 1967. On the description of anisotropic work hardening. J. Mech. Phys. Solids 15, 163–175.

Mroz, Z., 1969. An attempt to describe the behavior of metals under cyclic loads using a more general work-hardening model. Acta Mechanica 7, 199–212.

Mroz, Z., Shrivastava, H.P., Dubey, R.N., 1976. A non-linear hardening model and its application to cyclic loading. Acta Mechanica 25, 51–61.

McDowell, D.L., 1985a. A two surface model for transient nonproportional cyclic plasticity. Part I: development of appropriate equations. Journal of Applied Mechanics, ASME 52, 298–308.

McDowell, D.L., 1985b. A two surface model for transient nonproportional cyclic plasticity. Part II: comparisons of theory with experiments. Journal of Applied Mechanics, ASME 52, 307–315.

Ohno, N., 1982. A constitutive model of cyclic plasticity with a nonhardening strain region. Journal of Applied Mechanics, ASME 49, 721–727.

Ohno, N., Takahashi, Y., Kuwabara, K., 1989. A constitutive modeling of anisothermal cyclic plasticity of 304 stainless steel. Journal of Engineering Materials and Technology 111, 106–114.

Ohno, N., 1990. Recent topics in constitutive modeling of cyclic plasticity and viscoplasticity. App. Mech. Rev., ASME 43 (11), 283–295.

Ohno, N., Wang, J.D., 1991a. Transformation of a nonlinear kinematic hardening rule to a multisurface form under isothermal and nonisothermal conditions. International Journal of Plasticity 7, 879–891.

Ohno, N., Wang, J.D., 1991b. Two equivalent forms of nonlinear kinematic hardening: application to nonisothermal plasticity. International Journal of Plasticity 7, 637–650.

Ohno, N., Wang, J.D., 1993a. Kinematic hardening rules with critical state of dynamic recovery, part I: formulation and basic features for ratcheting behavior. International Journal of Plasticity 9, 375–390.

Ohno, N., Wang, J.D., 1993b. Kinematic hardening rules with critical state of dynamic recovery, part II: application to experiments of ratcheting behavior. International Journal of Plasticity 9, 391–403.

Ohno, N., Wang, J.D., 1994. Kinematic hardening rules for simulation of ratcheting behavior. European Journal of Mechanics 13, 519–531.

Ohno, N., 1997. Recent progress in constitutive modeling for ratcheting. Materials Science Research International 3 (1), 1–9.

Prager, W., 1956. A new method of analyzing stresses and strains in work-hardening plastic solids. Journal of Applied Mechanics, ASME 23, 493–496.

Phillips, A., Tang, J.L., Ricciuti, M., 1974. Some new observations on yield surfaces. Acta Mechanica 20, 23–39.

Phillips, A., Weng, G.J., 1975. An analytical study of an experimentally verified hardening law. Journal of Applied Mechanics, ASME 42, 375–378.

Phillips, A., Lee, C.W., 1979. Yield surfaces and loading surfaces. Experiments and recommendations. International Journal of Solids and Structures 15, 715–729.

Phillips, A., Lu, W.-Y., 1984. An experimental investigation of yield surfaces and loading surfaces of pure aluminum with stress-controlled and strain-controlled paths of loading. Journal of Engineering Materials and Technology, Trans. ASME 106, 349–354.

Shiratori, E., Ikegami, K., Yoshida, F., 1979. Analysis of stress-strain relations of use of anisotropic hardening potential. Journal of the Mechanics and Physics of Solids 27, 213–229.

Sivakumar, M.S., Voyiadjis, G.Z., 1997. A simple implicit scheme for stress response computation in plasticity models. Computational Mechanics 20, 520.

Tanaka, E., Murakami, S., Ooka, M., 1985. Effect of strain path shapes on non-proportional cyclic plasticity. J. Mech. Phys. Solids 33 (6), 559–575.

Tanaka, E., Murakami, S., Ooka, M., 1987. Constitutive modeling of cyclic plasticity in non-proportional loading conditions. In: Tucson, A.Z., Desai, C.S. (Eds.), Proc of the 2nd Int. Conf. on Constitutive Laws for Engineering Materials, Theory and Applications. Elsevier, New York, pp. 639–646.

Tseng, N.T., Lee, G.C., 1983. Simple plasticity model for two surface type. Journal of Engineering Mechanics, ASCE 109 (3), 795–810.

Voyiadjis, G.Z., Kattan, P.I., 1990. A generalized eulerian two-surface cyclic plasticity model for finite strains. Acta Mechanica 81, 143–162.

Voyiadjis, G.Z., Kattan, P.I., 1991. Phenomenological evolution equations for the backstress and spin tensors. Acta Mechanica 88, 91–111.

Voyiadjis, G.Z., Sivakumar, S.M., 1991. A robust kinematic hardening rule with ratcheting effects: part I. theoretical formulation. Acta Mechanica 90, 105–123.

Voyiadjis, G.Z., Sivakumar, S.M., 1994. A robust kinematic hardening rule with ratcheting effects: part II. Application to nonproportional loading cases. Acta Mechanica 107, 117–136.

Voyiadjis, G.Z., Basuroychowdhury, I.N., 1998. A plasticity model for multiaxial cyclic loading and ratchetting. Acta Meahanica 126, 19–35.

Voyiadjis, G.Z., Kattan, P.I., 1999. Advances in Damage Mechanics: Metals and Metals Matrix Composites. Elsevier, Oxford.

Wang, H., Barkley, M.E., 1998. Strain space formulation of the Armstrong-Fredrick family of plasticity models. ASME J. Eng. Mat. Tech. 120 (3), 230–235.

Wang, H., Barkley, M.E., 1999. A strain space nonlinear kinematic hardening/softening plasticity models. International Journal of Plasticity 15, 755–777.

Yoshida, F., Uemori, T., Fujiwara, K., 2002. Elastic-plastic behavior of steel sheets under in-plane cyclic tension-compression at large strain. International Journal of Plasticity 18, 633–659.

Yaguchi, M., Yamamoto, M., Ogata, T., 2002. A viscoplastic constitutive model for nickel-base superalloy, Part I: kinematic hardening Rule of Anisotropic Dynamic Recovery. International Journal of Plasticity 18, 1083–1109.

Ziegler, H., 1959. A modification of Prager's hardening rule. Quart. Appl. Math. 7, 55–65.